A gradient-based multiaxial criterion for fatigue crack initiation prediction in components with surface roughness

Bjørn Skallerud[a] *, Sigmund Kyrre Ås[b], Niels S Ottosen[c]
[a] Norwegian University of Science and Technology, Department of Structural Engineering, 7491 Trondheim, Norway
[b] Norwegian University of Science and Technology, Department of Marine Technology, 7491 Trondheim, Norway
[c] Division of Solid Mechanics, Lund University, P.O. Box 118, SE-221 00 Lund, Sweden

Abstract

The current study presents methods to predict the governing crack initiation site and fatigue crack initiation life of components with surface roughness. The surface topography is measured with white light interferometry and explicitly accounted for in detailed finite element models. The micro-notch stress fields are used in multiaxial and uniaxial crack initiation criteria where the relative stress gradient is included. The numerical predictions are compared with test results for cylindrical aluminum specimens with axi-symmetric surface roughness. Damage parameters based on the average stress fields over a certain distance were found to be highest in the micro-notches where cracks grew to failure. Lifetime predictions using a multiaxial damage criterion with a gradient correction and elastic-plastic stress fields showed good correlation with the experiments. Uniaxial criteria, criteria without gradient correction, and criteria based on linear elastic stress fields were found to be overly conservative. In some specimens, the failure location could not be identified by the proposed damage criterion. This is likely due to the presence of microstructural weaknesses near the micro-notches, leading to shorter initiation lives that cannot be described by geometry alone. It is concluded that resolving the detailed surface topography and accounting for this geometry in a detailed finite element model provide a predictive approach when multiaxial stresses are accounted for, but the importance of microstructure needs further attention.

Keywords

Fatigue crack initiation, surface roughness, finite element methods, multiaxial damage, notch stress gradient

1 Introduction

For many mechanical and structural components a large part of the fatigue life consists of initiating a small crack. Engineering prediction approaches (Basquin and Manson-Coffin types) have been used extensively. A large effort has been put into understanding the fatigue damage

*Corresponding author. Mail: bjorn.skallerud@ntnu.no. Tel.: +47 73550303.

initiation mechanism in specimens with smooth surfaces, where it is shown that the extrusion-intrusion mechanism due to localized slip is a governing factor. In actual components, the surface usually has some level of roughness. Unless extremely careful polishing procedures are employed, a surface will have irregularities that can be considered as a large number of micro-notches. Such surfaces may be considered smooth from an engineering perspective, but are not smooth when compared to the finely polished components used in fundamental crack initiation studies. In order to account for surface roughness in fatigue life predictions one can employ correction factors, e.g., such as proposed by Juvinall(1967) and Siebel and Gaier (1956). The number of detailed studies on fatigue crack initiation from specimens with rough surfaces is small compared to the studies employing mirror polished surfaces (Ås et al., 2005, Ås et al., 2008, Suraratchai et al., 2008, Cheng et al., 2017). On the other hand, fatigue initiation in single notches with a well-defined geometry (holes, fillets, V-shapes) has been studied extensively. Important early contributions were provided by Neuber(1937) and Peterson(1959). As the understanding of short cracks evolved during the 1980s, these early attempts were recast into fracture mechanics concepts, particularly the short-crack threshold and conditions for non-propagating cracks (Miller 1982, Lukas et al. 1989). A few authors have applied these concepts for surface roughness, e.g. Suhr (1986), Taylor and Clancy (1991), Murakami (2002) and Ås (2006). Short-crack theories have also been considered when estimating equivalent stress concentration factors for rough surfaces (Andrews and Sehitoglu, 2000, Kleemann and Zenner, 2006, Arola and Williams, 2002).

Initiation from micro-notches is governed by short crack growth, thus it makes sense to apply this concept to determine the fatigue limit, which is dictated by the length of non-propagating cracks. However, in many engineering applications it is desirable to operate in the finite life regime, which poses some inherent challenges specific to short crack growth (McDowell, 1996). This is the motivation for the current study, where multiaxial damage criteria are used to predict the initiation fatigue life.

From a technical perspective, having quantitative methods to account for surface roughness in fatigue predictions are very important. As a prerequisite to account for surface roughness one needs accurate methods to determine the surface topography. Such methods have evolved over the last decades and the equipment is readily available today. Many of the methods use light and are based on non-contact scans (lasers, white light interferometry). The spatial resolution in some of these methods is in micrometer (and even nanometer) scale. This is sufficient to capture a wide range of roughness levels. A map of the surface topography can be used as input to numerical tools such as finite element methods and crystal plasticity finite element methods (CPFEM). An application of surface mapping was provided by Ås et al. (2005), where white light interferometry (WLI) was used to find the surface geometry of cylindrical Al 6082-T6 specimens. Detailed finite element analyses accounting for the actual surface of each test specimen were carried out. The roughness was also characterized by geometric parameters such as the widely used average roughness, $R_z = \frac{1}{L}\int_L |z| dL$. The average roughness values for these specimens were in the range 2-11 μm, and maximum valley depth was in the range 10-51 μm. Such roughness measures do not tell anything about local valley curvature, i.e. the value may represent both a round or a very sharp micro-notch tip. WLI mappings can provide such information. Ås et al. (2008) provide a detailed description of how to establish the surface topography from WLI data points using cubic Bezier spline interpolations. This leads to smooth transitions between sample points and allows the meshing algorithm to refine the element size small enough to capture micro-notch stress fields. One can argue that using finite elements of micrometer size is violating the continuum assumption

since the elements are of same size as the microstructural elements and less than representative volume elements (RVE). In recent years, accounting for microstructure in fatigue crack inititation analyses has received increased focus, e.g., by CPFEM methods (McDowell, 2007, Bennet and McDowell, 2003, Manonukul and Dunne, 2004, Li et al., 2015, Hallberg et al., 2018). This can provide more details on fatigue damage processes and is very important for increased understanding of the crack intitation phenomenon. However, it is computationally demanding and cannot be considered as an engineering approach yet. Hence, it is of interest to study whether one can obtain deeper and useful information by means of traditional continuum finite element methods also. This is the scope of the present study.

In the current study, tools are developed to identify the governing notch. Knowing the most critical notch where fatigue failure initiated, the corresponding notch field can be employed with a damage criterion in order to estimate fatigue crack initiation life. The outline of the current study is as follows. First, the basic method for evaluation of fatigue crack initiation is presented. A simple analytic derivation is provided in the Appendix in order to investigate qualitative features of the approach. Second, the fatigue capacity for the smooth and rough specimens are presented. Detailed information of micro-notch depths and widths for the specimens are provided in Supplementary material. Third, the finite element results are processed to predict the fatigue crack initiation site and corresponding fatigue life. Finally, discussion and concluding remarks are provided.

2 Fatigue damage evaluation method

2.1 Observations from linear elastic analysis

The experimental procedure and finite element analyses are described in Ås et al. (2005, 2008). Cylindrical specimens with a diameter of 6.2 mm were machined from an extruded aluminium alloy 6082-T6, with chemical composition as shown in Table 1. Reference specimens were polished to a mirror finish. Specimens with surface roughness were produced by grinding in a lathe, where an emery paper pad was applied to the test section using a constant force while the specimen was rotated. The aim was to produce circumferential surface roughness so that axi-symmetric FE models could be used. To account for variations around the circumference, the specimens were measured using WLI at four hoop positions, denoted by clock values 0, 3, 6, and 9. Four 2D surface profiles were thus produced for each specimen, and these profiles were meshed and analyzed using scripts. Sub-surface stresses and strains were extraced for each significant notch, from the notch tip to a depth of 100 μm. Smaller valleys (perturbation less than 2 μm) were excluded by rainflow filtering. Since the surfaces were produced by different emery papers (80-120 grit size), the number of notches identified ranged from 50 to 180 for each surface profile. After fatigue failure, the fracture surface was investigated and the notch that governed the fatigue failure was identified using a stereo microscope. The hoop position of crack initiation was noted, thus the notch in the profile corresponding to the closest clock position was chosen as the initiation notch.

Fig. 1 shows an example for a specimen, using elastic finite element analysis. The axial loading was fully reversed (R=-1). Ten of the stress fields, corresponding to the highest stress concentrations, are colored and numbered. To the right the corresponding notch geometry and the axial stress at the surface are plotted. The white vertical line in these figures corresponds to the abscissae in the figure to the left. Notch number 8 is the one that governed the fatigue life. One notes that this notch does not give the largest stress at the notch tip (compared

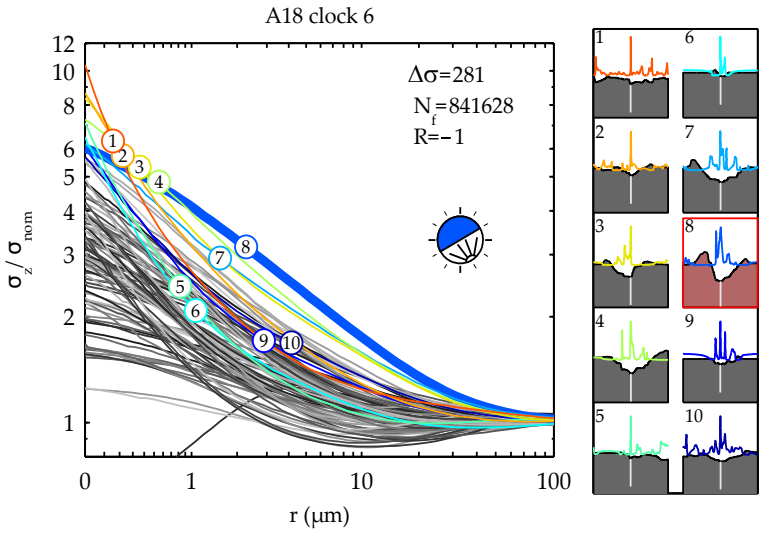

Figure 1: Example of notch stress fields due to surface roughness for one Al specimen

to notches 1-7,9,10). One also notes that the slope (gradient) of the stress field for notch 8 is not as steep as for the other nine notches. Interestingly, similar notch fields governing the fatigue life were found in most of specimens tested. One can hypothesize that for the most critical initiation notch, the fatigue damage is governed by a combination of the stress and strain at the tip and in some material domain in front of the tip. Already in 1937 Neuber in his classical book discussed sharp notches and effects of stress field gradient. Siebel and Pfender (1947) proposed to include the relative stress gradient into the fatigue assessment. Siebel and Stieler(1955) introduced the relative stress gradient in a modified version of the Neuber fatigue notch factor:

$$K_f = \frac{K_t}{1+\sqrt{cs}} \tag{1}$$

$$s = \frac{|(\partial\sigma_z/\partial r)_{notch}|}{\sigma_{z,notch}} \tag{2}$$

Here K_t is the elastic stress concentration factor, c is a fitting parameter of dimension length, σ_z is the axial stress, r is the radial distance from the notch tip, and s is the relative stress gradient at the notch tip.

2.2 Damage criterion

For a uniaxial stress state and elastic material, Siebel and Stieler (1955) proposed a fatigue life prediction method that accounts for a notch field stress gradient. If one considers the original set-up by Siebel and Stieler (1955), the prediction would read:

$$\begin{aligned} K_f &= \frac{\sigma_0}{\sigma_{0,notch}} = \frac{K_t}{1+\sqrt{cs}} \\ \Rightarrow \underbrace{K_t\sigma_{0,notch}}_{\sigma_{max}} &= \underbrace{\sigma_0(1+\sqrt{cs})}_{\sigma_{0,corr}} \Longleftrightarrow \sigma(r=0) = \sigma_0(1+\sqrt{cs(r=0)}) \end{aligned} \tag{3}$$

Here, $\sigma_{0,notch}$ is the nominal stress fatigue capacity for the notched component at the same number of cycles to failure as for a reference specimen. The reference fatigue capacity, σ_0, is the fatigue limit for fully reversed loading (R=-1) for a polished specimen without stress gradients. Then, according to Siebel and Stieler, the fatigue limit should be corrected to $\sigma_{0,corr} = \sigma_0(1 + \sqrt{cs})$ in case of stress gradients. Consequently, one should expect a higher fatigue limit if the specimen is subjected to a stress gradient (e.g., comparing a specimen loaded in tension or bending for the same maximum stress). Interpretation of this relationship shows that it is a single point evaluation of the notch field, carried out at the notch tip (i.e. $\sigma_z(r = 0)$ and $s(r = 0)$). The length parameter c is linked to the single point method (Eq. 3).

The stress fields near the notches in the cylindrical fatigue specimens are multiaxial. Hence, one should consider some multiaxial fatigue damage assessment. There are many multiaxial fatigue damage criteria available, ranging from simple invariant based (Crossland, 1956, Sines, 1959) to critical plane based (Fatemi and Socie, 1988, Dang Van, 1971, Papadopoulus et al., 1997). The latter criteria work well for non-proportional stress histories, where the influence of cyclic hardening/softening on damage evolution can be important (Skallerud, 1992). As the problems analyzed herein correspond to proportional loading and no out-of-phase stress histories, we will use the simple Sines criterion.

In the following we decompose the stress states in a constant mean and a cyclic amplitude such as $\boldsymbol{\sigma} = \boldsymbol{\sigma}_m + \boldsymbol{\sigma}_a \sin \omega t$. Further, consider the damage criterion

$$\beta = (\frac{3}{2}\mathbf{s}_a : \mathbf{s}_a)^{1/2} + B\mathrm{tr}(\boldsymbol{\sigma}_m) - \sigma_0 \leq 0 \qquad\qquad \mathbf{s}_a = \boldsymbol{\sigma}_a - \frac{1}{3}\mathrm{tr}(\boldsymbol{\sigma}_a)\mathbf{I} \tag{4}$$

where $\mathbf{s}$ is the deviatoric part of the stress tensor and $\mathrm{tr}(\cdot)$ is the trace of the tensor. The subscript "a" denotes amplitude. In a uniaxial stress state this reduces to the Haigh criterion, with B accounting for influence of mean stress on fatigue capacity. For an axisymmetric stress state and no stress gradients this reads

$$\begin{aligned} \beta &= \frac{1}{\sqrt{2}}[(\sigma_{az} - \sigma_{ar})^2 + (\sigma_{ar} - \sigma_{a\theta})^2 + (\sigma_{a\theta} - \sigma_{az})^2 + 6\sigma_{a,rz}^2]^{1/2} \\ &+ B(\sigma_{mr} + \sigma_{mz} + \sigma_{m\theta}) - \sigma_0 \\ &= \sigma_{ae} + B\mathrm{tr}\boldsymbol{\sigma}_m - \sigma_0 \leq 0 \end{aligned} \tag{5}$$

This is the Sines criterion (Sines, 1959). z denotes the longitudinal direction, θ is the circumferential direction. σ_{ae} is the amplitude of the equivalent stress. In the following, we combine this criterion with the corrected fatigue capacity $\sigma_{0,corr}$. The relative stress gradient is accounted for, generalized to multiaxial situations. Ottosen et al. (2018) proposed the following:

$$s = \frac{\sqrt{\nabla\sigma_e \cdot \nabla\sigma_e}}{\sigma_e} \tag{6}$$

$$\sigma_e = \sqrt{\frac{3}{2}\mathbf{s} : \mathbf{s}} \tag{7}$$

In a uniaxial stress field, Eq. 6 reduces to $|\frac{\partial\sigma/\partial x}{\sigma}|$. We employ gradient corrections to the fatigue capacity due to the stress gradients in the surface roughness micro-notches. Using the finite element results, $\beta(r)$ can be calculated. Although this approach was developed for linear

elastic solutions, we found that better predictions could be obtained by using an elastic-plastic solution and a bi-linear kinematic hardening model fitted to the cyclic stress-strain curve.

An alternative approach based on strain gradients for the correction of the fatigue capacity is also employed, hypothesizing that the strain gradient is smoother than the stress gradient. The relative strain gradient is defined as

$$s_\epsilon = \frac{\sqrt{\nabla\epsilon_e \cdot \nabla\epsilon_e}}{\epsilon_e} \tag{8}$$

$$\epsilon_e = \sqrt{\frac{3}{2}\mathbf{e}:\mathbf{e}} \qquad \mathbf{e} = \boldsymbol{\epsilon} - \frac{1}{3}\mathrm{tr}(\boldsymbol{\epsilon})\mathbf{I} \tag{9}$$

ϵ_e is the equivalent total strain. With this, $s_\epsilon \to s$ for vanishing plasticity. Now we have several possible simplifications that also can be investigated. From Eq. 5 the multiaxial, gradient corrected damage evaluation (for R=-1)reads

$$\beta = \sigma_{ae} - \sigma_{0,corr} = 0 \tag{10}$$

Alternatives to this is: 1) neglect the gradient correction:

$$\beta = \sigma_{ae} - \sigma_0 = 0, \tag{11}$$

or 2) only account for the longitudinal stresses σ_z:

$$\beta = \sigma_{az} - \sigma_{0,corr} = 0, \tag{12}$$

or 3) use the longitudinal stress and neglect the gradient correction:

$$\beta = \sigma_{az} - \sigma_0 = 0. \tag{13}$$

When Eq. 11 is averaged over a distance (see next section), we obtain the classical critical distance method (Taylor, 1999). Some studies assume that the axial stress governs the fatigue crack inititation. This is represented by Eq. 13. Eq. 12 is a variant of the others. The relative performance of these criteria is evaluated in Section 3.3.

2.3 Notch field averaging schemes

Inspired by the theory of critical distance (Taylor, 1999), we hypothesize that fatigue initiation life is governed by the stress field ahead of the notch. Knowing the uncracked specimen fatigue limit, σ_0, and the crack growth threshold value ΔK_{th} (both measured at the same R-ratio), one finds the transition between fatigue capacity for the smooth and the cracked specimen: $a_0 = \frac{1}{\pi}(\frac{\Delta K_{th}}{\Delta\sigma_0})^2$ (the largest non-propagating crack) (Kitagawa and Takahashi, 1976, El Haddad et al., 1979). According to Taylor (1999) the critical length to use in averaging the stress field is $L = 2a_0$. This is an application of the Neuber method. If a point method is employed, $L = a_0/2$. This corresponds to Peterson's approach. In prediction of the fatigue life of the notched specimen, one usually calculates the average stress $\sigma_{av} = \frac{1}{L}\int_L \sigma(r)dr$, and equates this to the unnotched material fatigue limit as a criterion for fatigue crack initiation, i.e. $\sigma_{av} = \sigma_0$. A detailed discussion of the feasibility of this method is provided by Susmel (2008). There also some open questions are given. Härkegård and Halleråker (2010) provide an interesting comparison of different averaging schemes. Tovo and Livieri (2008) provide

alternative ways of discretizing and averaging notch stress fields. In the current study a somewhat different method is employed, where the damage criterion β is averaged over a distance. Hence, both the equivalent stress field and the fatigue limit corrected for the stress (or strain) gradient are averaged. In the current study we use the critical distance $L = 2a_0$ as the averaging length for the notch fields, i.e. $\overline{\beta} = \frac{1}{L}\int_L \beta(r)dr$. Hence, using L and $\Delta L = L/n$ in the discretization of the fields, we have:

$$\begin{aligned}
\overline{\sigma}_{ae} &= \frac{1}{n}\sum_{i=1}^{n}\sigma_{ae}(r=(i-1)\frac{L}{n}) = \frac{1}{n}\sum_{i=1}^{n}\sigma_{ae}(r_i) && (14)\\
\overline{\sigma}_{0,corr} &= \sigma_0\frac{1}{n}\sum_{i=1}^{n}(1+\sqrt{\frac{L}{n}s(r=(i-1)\frac{L}{n})}) = \sigma_0(1+\frac{1}{n}\sum_{i=1}^{n}\sqrt{\frac{L}{n}s(r_i)}) \\
&= \sigma_0(1+\overline{\sqrt{\Delta L s(r)}}) && (15)\\
\Rightarrow \overline{\beta} &= \overline{\sigma}_{ae} - \overline{\sigma}_{0,corr} \leq 0 && (16)
\end{aligned}$$

The overbars mean averaged values. Eq. 16 is the discretized and averaged version of the single point approach in Eq. 3 . This averaging scheme can then be used with the simplified expressions for β in Eqs. 11 , 12, 13. The influence of the discretization parameter n is discussed subsequently. We employ the elastic-plastic notch field with the above discretization and find the average β over L. Use of elastic-plastic notch fields has been proposed by Pluvinage and co-workers, see e.g. Qylafku et al. (1999).

2.4 Fatigue crack initiation life prediction

The damage criterion is based on the smooth specimen fatigue limit, in our case defined as the stress amplitude corresponding to $2 \cdot 10^6$ cycles. This means that the criterion gives a value $\overline{\beta} = 0$ at the fatigue limit. To provide an initiation criterion in the finite life regime, stresses above the fatigue limit should also be considered, leading to a $\overline{\beta} > 0$. Hence, the fatigue capacity should be adjusted in order to achieve $\overline{\beta} = 0$. Consider the following situation, corresponding to higher loading than that representing the fatigue limit:

$$\begin{aligned}
\overline{\beta} &= \overline{\sigma}_{ae} - \sigma_0(1+\overline{\sqrt{\Delta L s}}) = \alpha > 0 && (17)\\
\overline{\beta}_{finite} &= \overline{\sigma}_{ae} - \sigma_0(1+\overline{\sqrt{\Delta L s}}) - \alpha = \overline{\sigma}_{ae} - (\sigma_0 + \underbrace{\frac{\alpha}{1+\overline{\sqrt{\Delta L s}}}}_{\alpha^*})(1+\overline{\sqrt{\Delta L s}}) = 0 && (18)
\end{aligned}$$

Here, α is the the computed value of $\overline{\beta}$ used in order to adjust the fatigue capacity to the finite life region. Hence, α^* is the amount the fatigue limit needs to be corrected in order to make the damage criterion become zero. Now we can combine the adjusted (finite life) fatigue capacity $\sigma_{0,finite} = \sigma_0 + \alpha^*$ with the smooth specimen SN-curve to predict the fatigue life of the components with surface roughness:

$$\sigma_{0,finite} = K \cdot N^P \rightarrow N = (\sigma_{0,finite}/K)^{(1/P)} \quad (19)$$

This approach is employed subsequently.

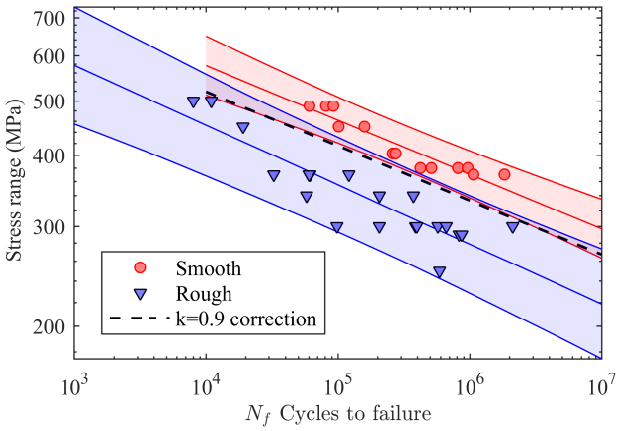

Figure 2: Stress range versus number of cycles to failure for the smooth and rough specimens (R=-1).

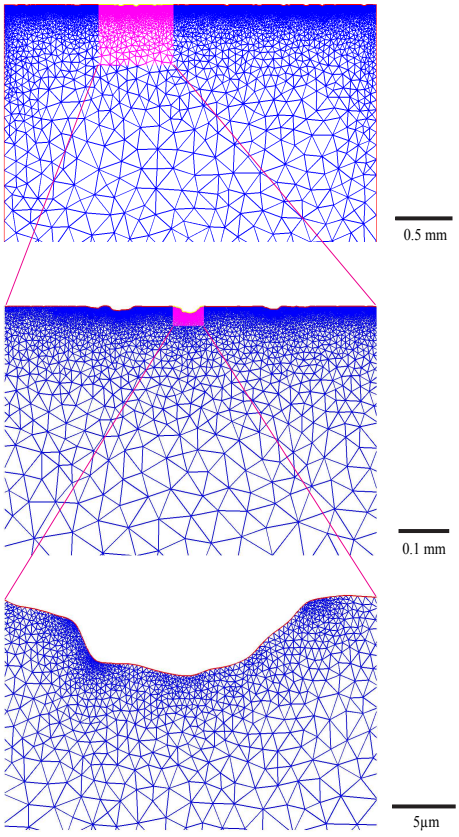

Figure 3: Mesh at a surface notch.

Table 1: Chemical composition of the material (wt.%)

Si	Fe	Cu	Mn	Mg	Cr	Zn	Ti	Other
1.16	0.29	0.091	0.53	0.81	0.14	0.069	0.028	0.10

Table 2: Fatigue lives and corresponding depth and width for the initiation micro-notch.

Specimen	$\Delta\sigma$ (MPa)	N	N_i	Depth (μm)	Width (μm)
X4	500	7997	1765	49.6	48.8
X26	500	10971	4739	35.1	81.2
X30	450	19188	10020	26.2	34.9
X9	370	32577	14106	32.6	52.3
X32	340	57780	32918	37.1	58.5
X39	370	60123	41652	44.3	77.6
X27	370	61172	42701	41.6	67.9
X43	300	98417	59609	41.2	83.6
X22	370	121315	102844	34.6	96.1
X24	300	206460	167652	17.1	27.8
X25	340	206577	181715	38.9	56.1
X21	340	373546	348684	19.7	40.0
X29	300	387725	348917	14.4	25.5
X40	300	395633	356825	35.4	65.4
X6	300	661827	623019	18.7	38.2
X28	290	870777	827022	30.2	70.4

2.5 Fatigue capacity of the specimens

Fig. 2 shows the stress versus total fatigue life results for smooth and surface roughened specimens. The mean regression lines are plotted along with the 5% and 95% prediction intervals. It is seen that the difference in fatigue capacity between smooth and rough specimens is very large. Also, the scatter increases significantly from smooth to rough specimens. One important observation is that even for the smooth specimens the scatter can be quite large, with a maximum difference on life approximately of a factor 5 for the lowest stress ranges. The spread increases to a factor 10 for the rough specimens. If we employ the measured average roughness R_z and employ an empirical correction curve such as presented by Juvinall, a reduction factor of approximately 0.9 is obtained. Adjusting the mean curve for smooth specimens with this factor, the black dashed line in Fig. 2 is obtained. The empirical correction will give non-conservative results for this alloy. It is noted that the slopes of the curves are close, indicating that the short crack growth stage has been overcome quickly due to the micro-notches. Table 2 lists the main data for the rough specimens: stress range, fatigue life, depth of the governing initiation notch, width of the notch at half of the depth. In Supplementary Material, micro-notch geometries for all specimens are provided.

The specimens were machined so that the loading direction is the same as the extrusion direction. The mean and median grain size perpendicular to the loading direction were 29 μm and 19 μm respectively, determined by electronic backscatter diffraction ($> 15^\circ$ crystallographic orientation mismatch). The grains were highly elongated in the extrusion (loading) direction, with lengths exceeding 2mm. The peak strength of this alloy in the T6 condition is due to Mg-Si precipitates of approximately 4x4x50 nm in size (Marioara et al., 2003). Larger precipitates, up to 3 μm in diameter, could be observed in a light microscope.

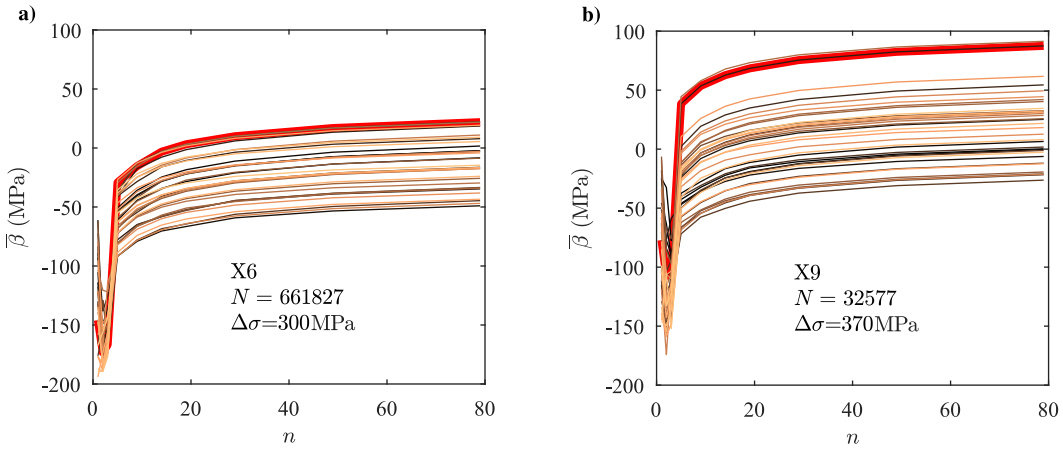

Figure 4: Sensitivity of $\overline{\beta}$ to number of segments used to discretize the notch field for a long-life specimen (a) and a short-life specimen (b).

The fracture surface of all specimens were microscopically investigated, and the crack growth was tracked back to its initiation point. Hence, this provided the initiation surface notch that governed the fatigue life. In the predictions presented below, $\overline{\beta}$ is calculated for all the micro-notches, and if the largest computed $\overline{\beta}$ corresponds to the initiation notch found in the microscope, the method is capable of predicting the intitiation site.

For long fatigue lives, the initiation fatigue life is about the same as the total life. For short fatigue lives, a significant part of the total life is spent in crack propagation. A simple adjustment of K and P in Eq.19 for the smooth specimens, removing some contribution from crack growth so they are more representative of initiation, is carried out. Initiation fatigue life N_i was calculated by subtracting the crack growth life N_p, from 0.5 mm to failure, from the total fatigue life as $N_i = N_{total} - N_p$. The crack length 0.5 mm was chosen as the shortest crack length that could be used for all stress levels while still adhering to linear elastic fracture mechanics. The full sigmoidal crack growth rate curve was used in conjunction with stress intensity factor solutions for an elliptical crack growing in a cylindrical bar. K and P (mean values) for the total fatigue life read $1.449{\cdot}10^3$MPa and -0.0986, respectively. The adjusted values (removing N_p) read $1.396{\cdot}10^3$MPa and -0.096.

The critical distance approach by Taylor is employed in order to determine the length in front of the notch where the β-field is averaged. For this aluminum alloy, the parameter a_0 (El Haddad et al., 1979) is found to be 16µm based on σ_0 for smooth specimens and ΔK_{th} (estimated from 6061-T6) for $R = -1$. Hence, the value for L in above equation is 32 µm. There are many alternative ways of deciding on this length: depth of notch (Morel et al., 2009), extent of notch field, distance from notch to where the stress field gradient changes sign (Qylafku et al., 1999), or some multiple of grain size (Amargier et al., 2010). In our case, the critical distance corresponds quite well to the governing initiation notch depth (Hallberg et al., 2018), extent of the notch field (Hallberg et al., 2018), grain size (Ås et al., 2005).

3 Finite element results

3.1 Post-processing of FE data

The FE analyses provide the stress and strain components for all of the notch fields. Details on the finite element modeling and meshing are provided in (Ås et al., 2008). Fig.3 shows an example of a mesh for a surface roughness notch. Axisymmetry and elastic-plastic material were employed. From the notch fields, we calculate the effective stress and strain along the r-axis. The nodal values are fitted to polynomial functions of order 5 using the Savitzky-Golay filtering in Matlab to smoothen the curves and provide high-quality derivatives for stress and strain. The sampling intervals must be constant with this filter, thus the original stress and strain solutions are resampled. The functions are then used in calculating the relative stress (and strain) gradients. From this the β-field is calculated. A fatigue limit $\sigma_0 = 190$MPa was employed, corresponding to the fatigue life of $2 \cdot 10^6$ cycles to failure for the mirror polished aluminum specimens (Ås et al., 2005). The critical distance for averaging the notch fields was estimated to be 32 μm. Then a value of n used in the discretization must be chosen. Fig. 4 shows how the average β evolves as a function of n for a large number of surface notches in two specimens. Specimen X9 has a fatigue life of $33{\cdot}10^3$ cycles to failure and specimen X6 has $660{\cdot}10^3$ cycles to failure, corresponding to a highly loaded and moderately loaded notch zone. The red line corresponds to the notch governing the fatigue intiation life. A coarse sub-division (e.g. n<20) gives a large variation of the computed $\overline{\beta}$. For n>30 the variation is low. In the following n=32 is chosen, i.e. $\Delta L = 1$μm is employed in Eq. 16.

Based on this approach, the first goal is to investigate whether $\overline{\beta}$ is a useful parameter that identifies the critical fatigue initiation notch.

3.2 Identifying the governing failure site

Figs 5 and 6 show computed notch fields for two specimens. The specimen in Fig. 5 (X6) has a relatively long fatigue life ($N = 661827$), about ten times longer than the specimen in Fig 6 (X39, $N = 60123$). The effective stress σ_{ae} is shown with the original FEA solution (dots) and the filtered interpolation lines. The calculated relative stress gradient s and corrected fatigue strength σ_0 are shown below, which enter into the calculation of β according to Eq. (10). The notch field corresponding to the notch causing the fatigue failure is highlighted in red. A rainflow counting method was used to filter out small notches, using 5μm as the smallest notch depth to be included in the evaluation of notch fields. The $\beta - r$ plots show a dominating trend: for almost all specimens the notch causing fatigue failure has the highest value of β. β-r represents a damage criterion field. In Fig. 7 $\overline{\beta}$ is reported for the specimens employing Eq.16 (i.e. multiaxial stresses and stress gradient accounted for). The upper part corresponds to specimens with a long fatigue life, the lower part corresponds to the low cycle fatigue region. The blue dots correspond to the computed $\overline{\beta}$ for the micro-notches, the red circles represent the governing initiation notch (identified from microscopy of the fracture surface). It is clear that the approach ranks the criticality of the different notches quite consistently. It was found that using relative strain gradients yielded similar results, or in some cases slightly worse identification compared to relative stress gradients. The results show that $\overline{\beta}$ has a feasible capability to identify the notch that governs the fatigue life, with exceptions for X24 and X29. It is noted that although there is a clear trend that the notch with the highest $\overline{\beta}$ corresponds to the critical notch (corresponding to the red circle), the computed value is close to zero only for the specimens with the longest fatigue lives. For

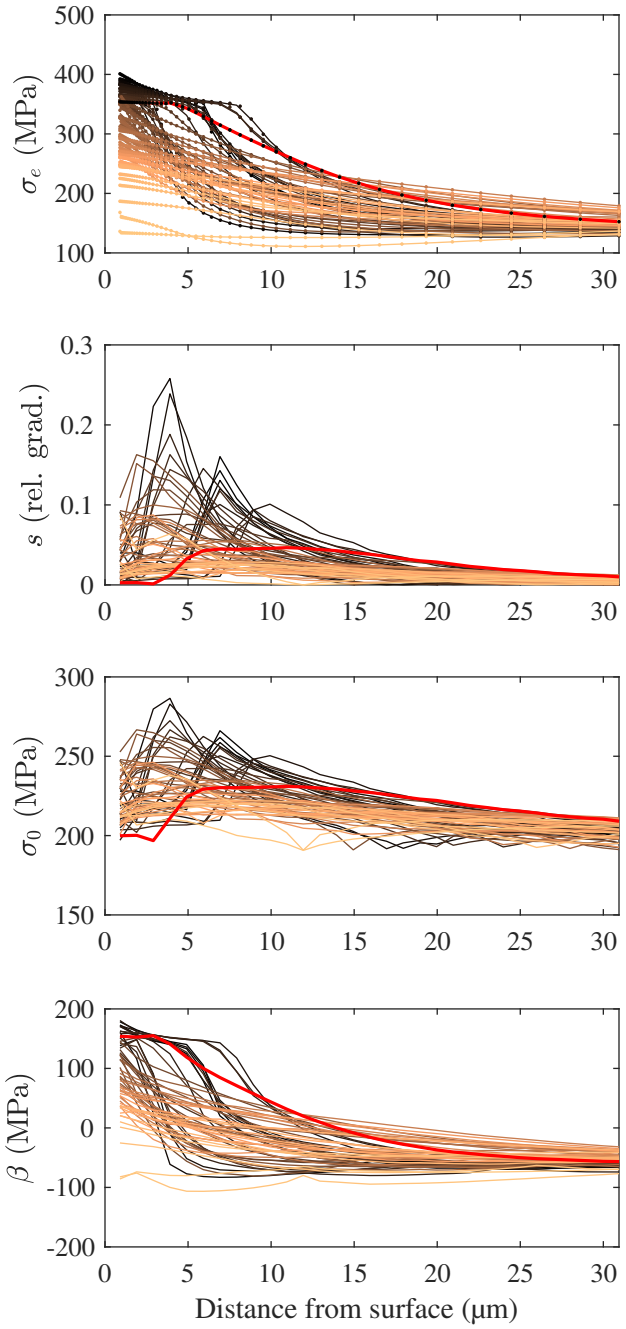

Figure 5: Notch fields for X6, elastic-plastic material.

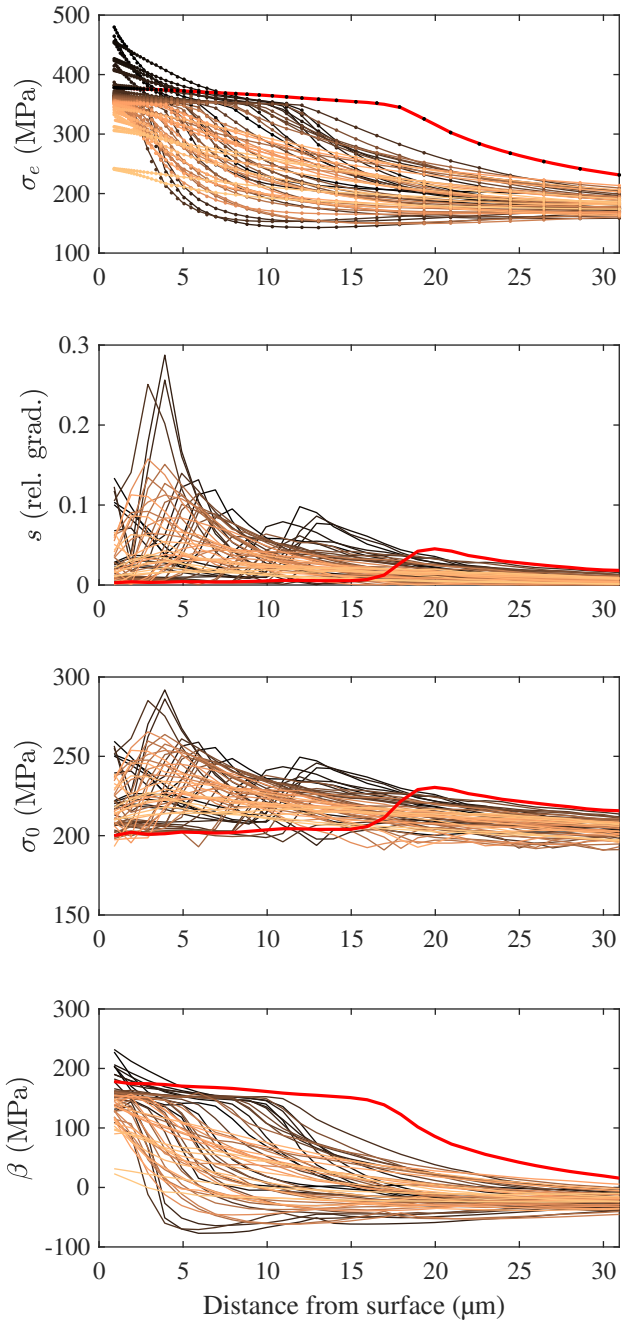

Figure 6: Notch fields for X39, elastic-plastic material.

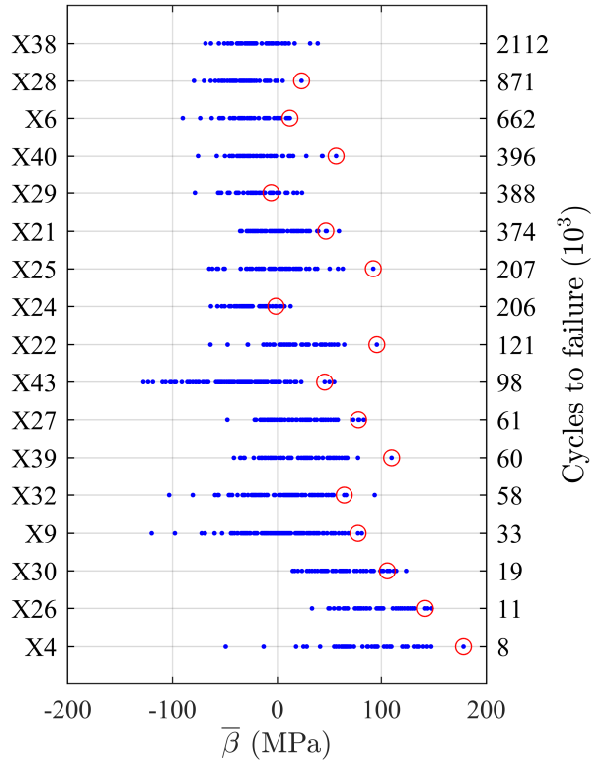

Figure 7: Average β based on elastic-plastic material for all specimens and all identified notches (note that X38 is a run-out). The red circles correspond to the initiation notch.

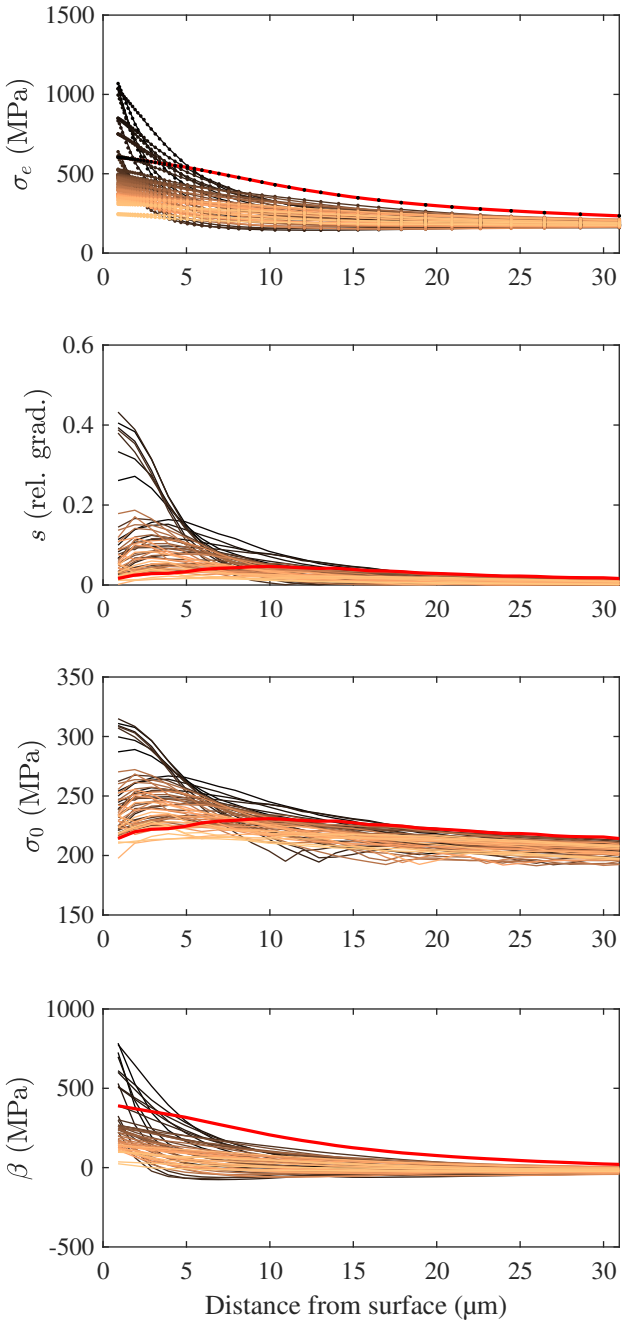

Figure 8: Notch fields for X39, linear elastic material.

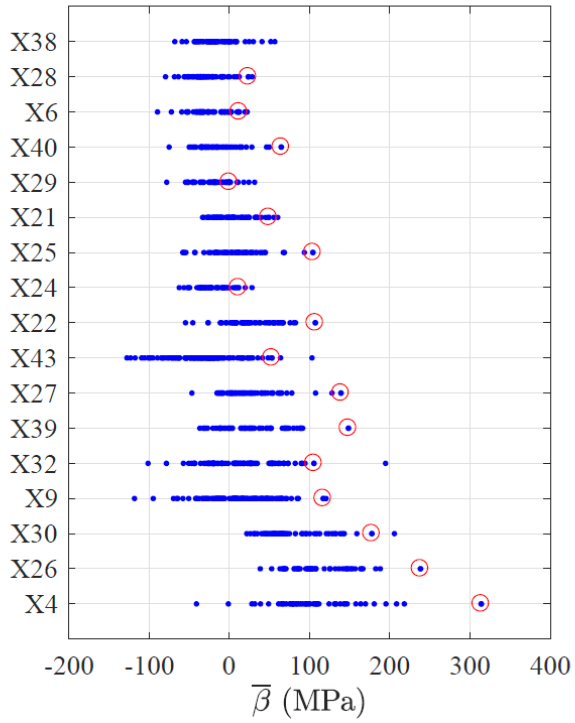

Figure 9: Average β based on linear elastic material for all specimens and all identified notches. The red circles correspond to the initiation notch.

higher loads, $\overline{\beta}$ is much larger than zero. This is to be expected as the basis for our fatigue capacity is based on the value corresponding to two million cycles, i.e. σ_0. For the criterion to match the test results, $\overline{\beta}$ should be zero for the most critical notch. Hence, if $\overline{\beta} \leq 0$, infinite fatigue life will be predicted, if $\overline{\beta} > 0$, the fatigue capacity is adjusted according to Eq.18 and the fatigue life predicted by Eq.19.

To simplify the approach, elastic analyses were also carried out. This violates the response of the material in the notch tip region, but if $\overline{\beta}$ still ranks the criticality of the surface notches it provides a simple engineering method. Fig 8 shows an example of elastic notch fields. Also the elastic $\overline{\beta}$ for each specimen is plotted in Fig. 9. The notch governing intitation is marked with a red circle. It is noted that even for elastic analysis, the approach ranks the criticality of the notches quite consistently.

Instead of using $\overline{\beta}$, the single point approach such as described by Eq. 3 was also tried for elastic and elastic-plastic material. In these cases the notch tip β did not rank the criticality of the notches well, and the governing intitation notch could not be identified. The likely reason for this is that the local stress value and gradient at the surface are very sensitive to geometric irregularities in the notch roots. While these type of criteria have been successfully used in well-defined notches with a given root radius, these results indicate that averaging criteria should be used in random topographies.

3.3 Fatigue crack initiation life prediction

As illustrated in the previous section, $\overline{\beta}$ was close to zero for the initiation notch for the longest fatigue lives and significantly larger than zero for the shorter fatigue lives. A remedy to obtain zero was presented in Section 2.4. The fatigue capacity mean curve for smooth specimens was employed and the fatigue limit σ_0 was adjusted to $\sigma_{0,finite}$. Using this approach, both for the SN-curve based on total fatigue life and the SN-curve based on a fatigue initiation life, the performance is obtained as shown in Fig. 10. The red circles correspond to the intitation SN-curve and the blue dots correspond to the total fatigue lives. It is noted that for the shorter lives, the difference between the pairs of red circles and blue dots is significant. For the long lives, this difference is almost negligible, illustrating the well known fact that for long lives, the fatigue life is dominated by initiation and for short lives the crack growth phase has a finite contribution to the total life. The predictions are mainly conservative. The blue triangles are based on predictions using the largest $\overline{\beta}$ calculated for the specimens in the cases where the value at the initiation notch was not the maximum. It is noted that e.g. the non-conservative predictions for X24 and X29 then improves.

Fig. 11 shows the performance of all of the evaluation criteria provided by Eqs. (10-13), where Eq. (10) accounts for multiaxial stresses and stress gradient (blue line) and Eq. (13) only employs the axial stress and no account for stress gradients (dashed yellow line). The mean life predictions become increasingly conservative the more simplifications one introduces in the damage criterion. The figure clearly demonstrates the importance of accounting for multiaxiality and stress gradients. Note that results using elastic material with Eq. (10) is also included (analogous to the results in Fig. 9). The linear elastic solutions (red line) provide reasonable predictions at long fatigue lives, and become increasingly conservative for shorter fatigue lives.

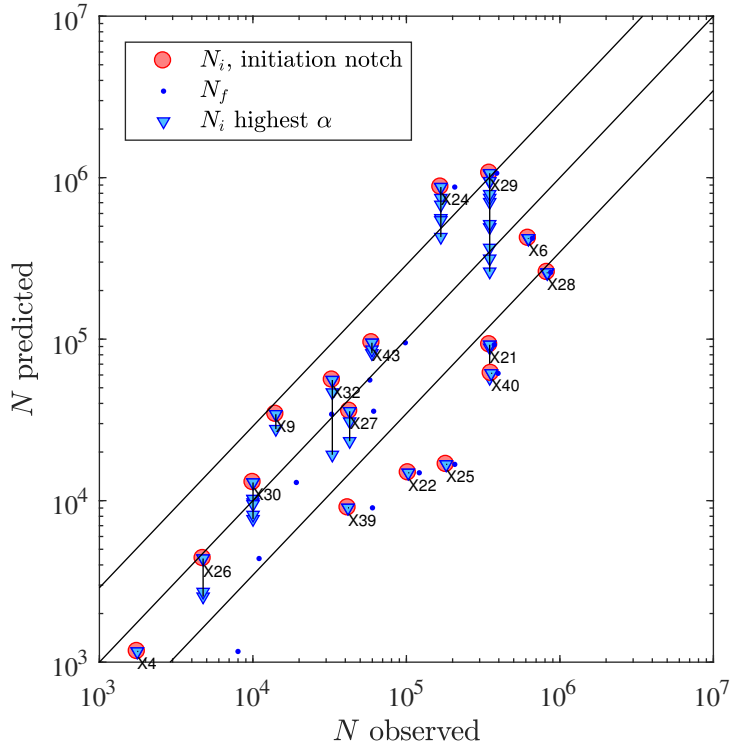

Figure 10: Comparison of predicted and observed fatigue lives. The red circles correspond to α values calculated for the initiation notch. Blue triangles correspond to notches with the highest α values, and also notches where α was higher than in the initiation notch.

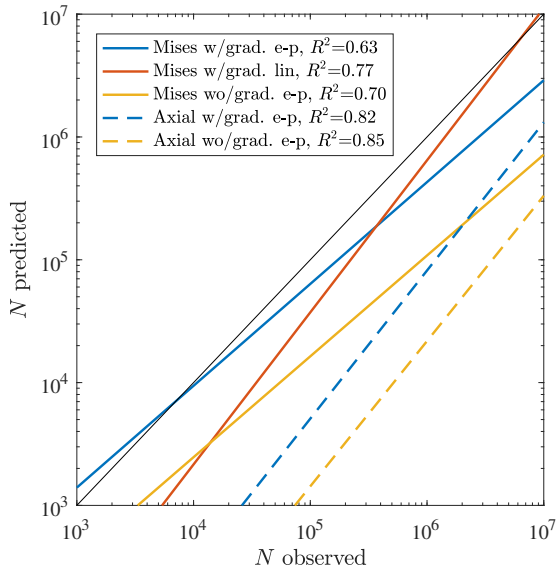

Figure 11: Life predictions, average curves for Eqs. (10, 11, 12, 13).

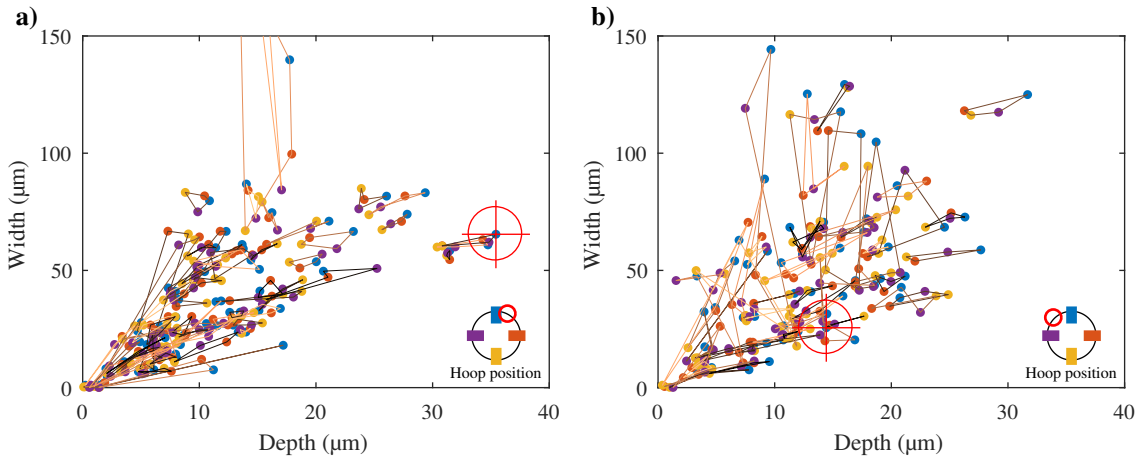

Figure 12: Relationship between depth and width (at half-depth) of notches for specimen X40 (a) and X29 (b). The initiation notch is marked by a cross hair. Colors refer to hoop positions as shown in the inset figure, where the exact initiation location is indicated by a circle. Lines connect the dots from the same notch.

4 Discussion

This study investigates the possibility of using continuum mechanics solutions in fatigue strength assessment of rough surfaces. The approach is verified both in terms of identifying the critical notch and fatigue life predictions. Compared to past studies based on average roughness, this approach is more quantitative and also provides finite life predictions as opposed to fatigue limit assessments. Figs. 5 and 6 show examples of notch fields for a moderately and a highly loaded specimen, respectively. The equivalent stress fields show a large variation over a short distance. This also leads to large variation in the relative stress (and strain) gradients, illustrating the need for a very detailed finite element mesh in the notch regions in order to capture this response. The notch stress fields are employed with a multiaxial fatigue criterion (Sines), and it is averaged over a critical distance (Taylor). Then the averaged fatigue damage criterion ($\overline{\beta}$) is obtained for hundreds of notches in each specimen. The hypothesis is that the $\overline{\beta}$ of highest value should correspond to the actual initiation notch. In most cases this turns out to be true. Two out of 16 cases show a deviation (X24 and X29, see Fig.7). For them there are several micro-notches that have a larger $\overline{\beta}$ than the notch that was found to govern the initiation. In Supplementary Material the depths and widths at half depth plots for all specimens are presented. The governing initiation notch is highlighted by a red cross. Looking at these for X24 and X29 shows that there are many notches that are deeper than the initiation notch. Hence, the computed $\overline{\beta}$ for these will be higher than for the initiation notch.

Considering the notch depths and widths for the remaining specimens, they all show that that the initiation notch depth is largest or in a group of the largest micro-notch depths. Hence, notch geometry plays a significant role in defining the initiation sites. Considering two examples of predictions of low accuracy, X29 is non-conservative and X40 is conservative (Fig. 10). They both are subjected to the same stress range $\Delta\sigma$=300 MPa and the experimental fatigue life is almost the same (390000 cycles). Figs. 12 and 13 show the distribution of notch depth and width and the detailed geometry of the respective initiation notches. The

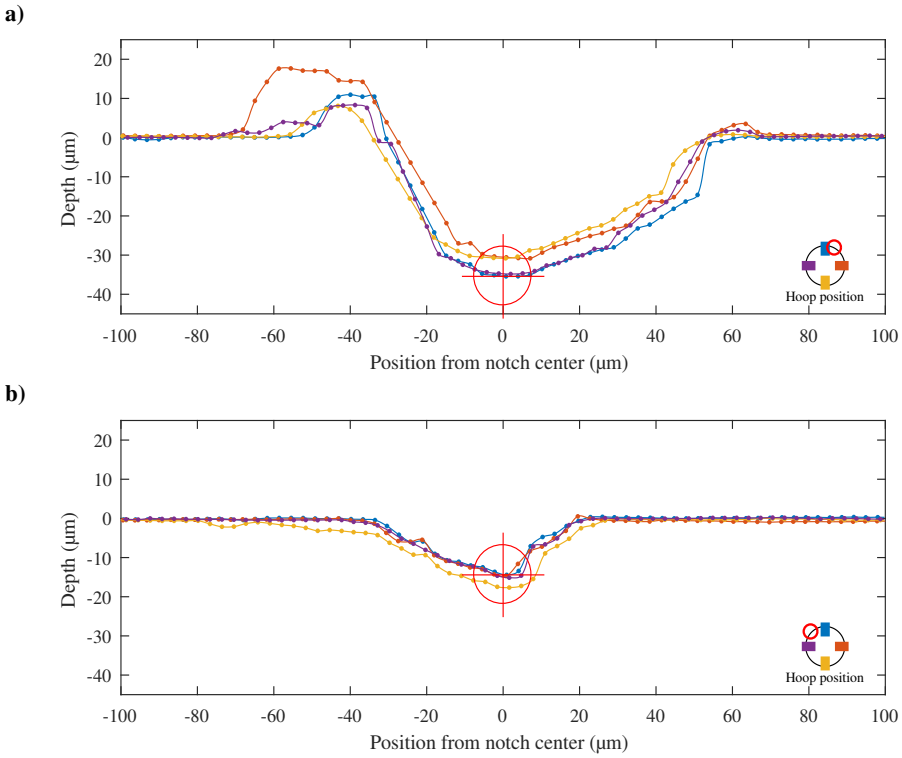

Figure 13: Area around the initiation notch for all measured hoop positions in specimen X40 (a) and X29 (b). Colors refer to hoop positions as shown in the inset figure, where the exact initiation location is indicated by a circle.

colors correspond to the notch geometry at the four different clock positions around the circumference. One notes that for X29 (Fig. 12b) there are many notches that are deeper than the intitation notch, for X40 the initiation notch is the deepest (Fig. 12a). Also, Fig. 13 shows that the geometry of the X29 initiation notch has a sharp V-shape, whereas for X40 it is a U-shape. The requirement of a finite element mesh in the notch region for the V-shaped notch of depth approximately 15μm would be higher than for the U-shaped notch of depth approximately 35μm. Hence, it is expected that the computed notch field for X29 is less accurate than for X40, and this affects the prediction. The notch field for the U-notch is expected to be calculated with higher accuracy than for the V-notch, and a good prediction should be possible to achieve. Reasons for this not being the case are discussed below.

Considering the non-conservative predictions in Fig. 10 (X24 and X29), it is noted that if we use the largest computed $\overline{\beta}$ in predicting the fatigue life, the accuracy improves significantly. This indicates that in an engineering assessment, one always use the largest $\overline{\beta}$. However, in addition to notch geometry, microstructure is important. The surface irregularities are of the same magnitude as the grain size of this aluminium alloy. Hallberg et al. (2018) analyzed with CPFEM two of the specimens analyzed by FEM herein (X22 and X40). The computational domain was 400μmx200μm, and 10 grains with different orientations obtained from ESBD measurements were analyzed. The stacking sequence of the grains of different orientations was permutated in order to investigate the importance of grain orientation (local slip) on the damage intitation below the notch. It was shown that whether the first grains near the notch tip have a favourable or unfavourable orientation has a large influence on computed damage parameters. Linking this information to the present FEM study, as we do not account for grain properties in our continuum models, we will have situations where the computed $\overline{\beta}$ for the initiation notch is lower than at other sites and due to a unfavourable grain orientation, the crack initiation still occurs here. We can also have a situation where the deepest notch identifies the governing notch even for a favourable grain orientation at this notch tip. Furthermore, we can have the deepest notch with an un-favourable grain orientation, leading to a fatigue life lower than that predicted by a continuum based approach. Hence, an important reason for the deviation between a continuum approach and a micromechanical approach is due to microstructural characteristics. Still, Fig. 7 shows that the present continuum approach provides useful information on identifying the governing initiation sites. Also, Fig. 9 indicates that purely elastic analyses can be used, which is convenient in engineering analyses.

This study presents an engineering assessment of fatigue crack initiation life. We chose to use an initiation crack size of 0.5mm. With this we could remove some of the crack growth life from the total fatigue life SN-curve, based on linear elastic fracture mechanics methods and long crack growth data. How to decide on what crack size defines the initiation phase is not trivial. A stricter choice would be of magnitude a few grains (e.g., 3 times average grain size$\approx$ 90μm for our material). Then the notch stress and/or strain field could be employed in a damage parameter to predict the initiation life corresponding to $a_i = 90$μm. Subsequent damage could be be calculated by a short crack growth evolution model. In engineering, when applying an SN-curve approach, one usually accepts that the SN-curve also consists of some crack propagation. We also do that in the current study. An initiation crack of 0.5mm is small for a thick component, and may well be a good measure for the initiation life. For thin components, this may not be true and may call for a smaller crack definition and require more advanced methods for prediction of short crack growth.

Several studies have shown that the plastic strain amplitude is governing the initiation

phase and the phase of short crack propagation, both in low cycle and high cycle fatigue (Tomkins, 1968, Ibrahim and Miller, 1979, Polák, 2005). If one carries out the tests under plastic strain amplitude control (and not stress amplitude control as in our case) one may address the problem of fatigue crack initiation life prediction with more advanced methods. E.g., the plastic strain amplitude or some equivalent plastic strain measure evolving in the notch fields may be alternative damage parameters. This is an interesting topic for further research.

Residual stresses influence the fatigue life. The residual stresses at the specimen surfaces were measured by X-ray diffraction, and surface stress level was approximately -150MPa for both rough and smooth specimens. When the surface roughness was generated by grinding, additional local residual stresses are introduced that makes the local stress situation at the micro-notches complicated (and unknown). One can obtain some information from the literature on evolution of residual stresses during fatigue testing. Prasannavenkatesan and McDowell(2010) investigated relaxation of compressive residual stresses introduced by shot peening, using CPFEM. They showed that during the first cycle a significant reduction is obtained (almost 30%) for nominal elastic high cycle fatigue loading at R=-1. This is caused by local grain orientations that are favourable for microslip. Considering our specimens, with micro-notches typically of depths 15-40micrometer, a cyclic plastic zone is present in the notch region. This local cyclic plasticity will affect and relax the local residual stress field. In future work one should try to measure as accurately as possible the local residual stress field and combine this with e.g. CPFEM in order to calculate the cyclic evolution of the residual stress and investigate how this affects local fatigue damage parameters.

A simple fatigue life prediction approach was suggested. As an initial fatigue capacity, the fatigue limit (or in our case the fatigue capacity corresponding to $2 \cdot 10^6$ cycles) was employed when computing $\overline{\beta}$. For higher load levels and shorter lives, this capacity was adjusted based on the smooth specimen SN-curve. The predicted lives showed mainly acceptable correspondence with test results, but a few conservative and un-conservative results were also obtained. As discussed above regarding influence of microstructure, it seems that micro-notches of size similar to the grain structure leads to a very demanding problem to solve.

5 Concluding remarks

In this study a method to identify the governing fatigue crack initiation site for specimens with surface roughness has been presented. Detailed finite element simulations of the micro-notch fields were the basis for the analysis. A Sines-based damage criterion was employed, where the fatigue capacity was adjusted for notch field gradients. The critical distance method was employed and the damage parameter was averaged over this length. Both elastic-plastic stress fields and elastic stress fields were applied, and both approaches worked well in identifying the initiation site. A simple approach to fatigue life prediction was tried. Reasonable predictions were obtained, and for the non-conservative cases, a detailed discussion of possible causes was provided. The current FE-based approach provides a more quantitative engineering method to account for surface roughness than previously proposed. However, microstructural features, such as grain orientation and other characteristics, are not accounted for in this continuum approach. Hence, an important feature is not considered in the model. Local micro-notch geometry is accounted for, but as the surface roughness notches are of same magnitude as grain size, one needs to employ more advanced methods (e.g. CPFEM) in order to account for microstructure. This has potential to further derive more quantitative methods for fatigue

crack intitation life predictions.

Acknowledgment

The authors would like to express their gratitude to Prof. M. Ristinmaa and Assoc. Prof. H. Hallberg for helpful discussions.

Appendix. Analytic results

An analytic approach is presented in order to do qualitative evaluations. We use the above methodology for a wide elastic plate with a circular hole and investigate how the damage criterion β evolves as function of hole diameter under plane stress. In typical notch analysis, the notch size is of magnitude mm or above, and the gradients are moderate. In our case the notch size is much smaller, and the evolution of β in such cases has not been investigated. β will be analysed by means of $d\beta/dr$. If the derivative is negative at the notch tip β must be a decreasing function of r, i.e. the notch tip is the most critical point for fatigue crack initiation. If the derivative is positive, β will increase and reach some maximum somewhere away from the notch tip inside the material. Employing the results from Timoshenko(1951) the stress along the r-axis in a plate with a circular hole of radius R, subjected to a nominal stress σ_{nom}, reads

$$\sigma_r = \frac{\sigma_{nom}}{2}(3\frac{R^2}{r^2} - 3\frac{R^4}{r^4}) \tag{20}$$

$$\sigma_z = \frac{\sigma_{nom}}{2}(2 + \frac{R^2}{r^2} + 3\frac{R^4}{r^4}) \tag{21}$$

The shear stress along the symmetry line is zero. Using this in the von Mises equivalent stress leads to

$$\sigma_e = \frac{\sigma_{nom}}{2}(4 - 2\frac{R^2}{r^2} + 25\frac{R^4}{r^4} - 18\frac{R^6}{r^6} + 27\frac{R^8}{r^8}) \tag{22}$$

Differentiating with respect to r, the stress gradient and the relative stress gradient (s) are obtained:

$$d\sigma_e/dr = \frac{\sigma_{nom}^2}{2\sigma_e}(\frac{R^2}{r^3} - 25\frac{R^4}{r^5} + 27\frac{R^6}{r^7} - 54\frac{R^8}{r^9}) \tag{23}$$

$$s = \frac{|d\sigma_e/dr|}{\sigma_e} = \frac{\sigma_{nom}^2}{2\sigma_e^2}(-\frac{R^2}{r^3} + 25\frac{R^4}{r^5} - 27\frac{R^6}{r^7} + 54\frac{R^8}{r^9}) \tag{24}$$

Now Sines criterion is employed, accounting for influence of stress gradient on the fatigue capacity:

$$\frac{d\beta}{dr} = \frac{d\sigma_e}{dr} - \sigma_0\sqrt{c}\frac{d(\sqrt{s})}{dr} \tag{25}$$

At the notch tip $\sigma_e = 3\sigma_{nom}$ and $d\sigma_e/dr = -\frac{17\sigma_{nom}}{2R}$. Furthermore, $s_{r=R} = \frac{17}{6R}$ and $(ds/dr)_{r=R} = -\frac{65}{9R^2}$. This leads to the following expression for the derivative of β at the notch tip:

$$(\frac{d\beta}{dr})_{r=R} = -\frac{17\sigma_{nom}}{2R} + 2.145\sigma_0\sqrt{c}\frac{1}{R^{3/2}} \tag{26}$$

Some qualitative features are obtained by plotting this equation as function of notch radius. $\sigma_0 = 150MPa$ is chosen. The material parameter $\sqrt{c}$ is set to typical values and the nominal stress amplitude is set to 150MPa or 75MPa. From Fig. 14 one observes that for very small notches (e.g., less than 80μm) the slope of β can be positive, indicating that β can be larger at some distance from the notch tip. This indicates that the fatigue damage also is a result of damage evolving in the interior. Comparing the two nominal stress levels, for the same c-value, a lower nominal stress amplitude gives a larger range with a positive slope. Comparing results for a constant stress amplitude, and varying c, one notes that the smaller the c, the more likely the notch tip will be the most critical location. For larger notch radii, the curves approach asymptotes with negative values. I.e., for typical finite sized notches of magnitude mm and above, the notch tip will be the most likely location for fatigue crack initiation according to the criterion employed.

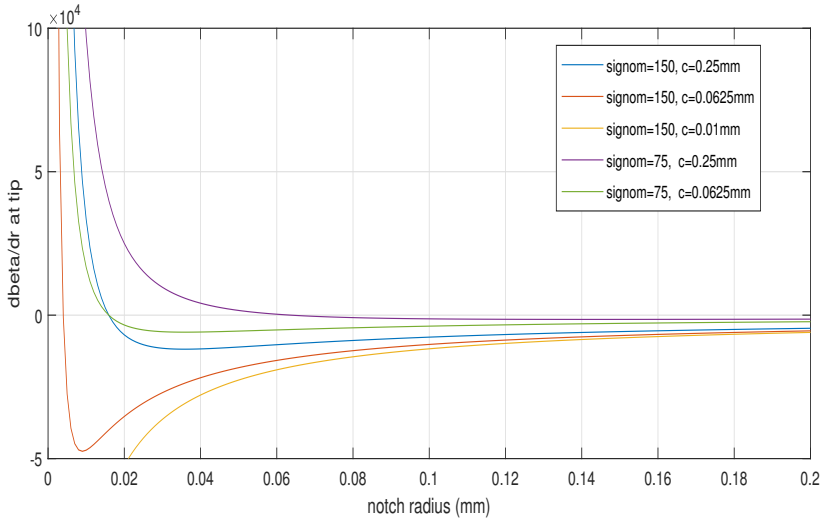

Figure 14: Sensitivity of the derivative of β (MPa/mm) at notch tip as function of the notch radius.

References

Amargier R, Fouvry S, Chambon L, Scwob C, Poupon C. Stress gradient effect on crack initiation in fretting using a multiaxial fatigue framework. Int J Fatigue 2010; 32; 1904-1912.

Andrews S, Sehitoglu H. A computer model for fatigue crack growth from rough surfaces, International Journal of Fatigue, 2000, 22, 619-630.

Arola D, Williams C. Estimating the fatigue stress concentration factor of machined surfaces, International Journal of Fatigue, 2002, 24, 923-930.

Bennett VP, McDowell DI. Polycrystal orientation distribution effects on microslip in high cycle fatigue. Int J Fatigue 2003; 25; 27-39.

Crossland B. Effect of large hydrostatic pressures on torsional fatigue strength of an alloy steel. In: Proc of the intern conf fatigue metals, London 1956; 138-149.

Dang VK. Sur la resistance a la fatigue des metaux. PhD thesis 1971, Univ Paris VI.

El Haddad MH, Topper TH, Smith KN. Prediction of non propating cracks. Eng Fract Mech 1979; 11; 573-584.

Fatemi A, Socie DF. A critical plane approach to multiaxial fatigue damage including out-of-phase loading. Fatigue Fract Eng Mater Struct 1988; 11; 149-165.

Hallberg H, Ås SK, Skallerud B. Crystal plasticity modeling of microstructure influence on fatigue crack initiation in extruded Al 6082-T6 with surface irregularities. Int J Fatigue 2018; 111; 16-32.

Härkegård G, Halleråker G. Assessment of methods for prediction of notch and size effects at the fatigue limit based on test data by Bøhm and Magin. Int J Fatigue 2010; 32; 1701-1709.

Ibrahim MFE, Miller KJ. Determination of fatigue crack initiation life. Fatigue & Fracture of Engineering Materials & Structures, 1979, 2, 351-360.

Juvinall RC. Engineering considerations of stress, strain, and strength. MCGraw-Hill, 1967.

Kitagawa H, Takahashi S. Applicability of fracture mechanics to very small cracks or the cracks in the early stage. Proc 2. Int Conf Mech Beh Mater 1976; 627-631.

Li L, Shen K, Proust G. Fatigue crack initiation life prediction for aluminium alloy 7075 using crystal plasticity finite element simulation. Mech Mater 2015; 81; 84-93.

Lukas P, Kunz L, Weiss B, Stickler R. Notch size effect in fatigue, Fatigue and Fracture of Engineering Materials and Structures, 1989, 12, 175-186.

Manonukul A, Dunne FPE. High and low cycle fatigue crack initiation using polycrystal plasticity. Proc Roy Soc Lond A 2004; 460; 1881-1903.

Marioara CD, Andersen SJ, Jansen J, Zandbergen HW. The influence of temperature and storage time at RT on nucleation of the β'' phase in a 6082 Al-Mg-Si alloy. Acta Materialia, 2003, 51, 789-796.

McDowell DL. Basic issues in the mechanics of high cycle metal fatigue, International Journal of Fracture, 1996, 80, 103-145.

McDowell DL. Simulation-based strategies for microstructure-sensitive fatigue modeling. Mater Sci Eng A 2007; 468-470; 4-14.

Murakami Y. Metal Fatigue: Effects of small defects and nonmetallic inclusions, Elsevier, 2002.

Neuber H. Theory of notch stresses. 2nd edition, Spronger Verlag 1958.

Ottosen NS, Ristinmaa M, Kouhia R. Enhanced multiaxial fatigue criterion that considers stress gradient effects. Int J Fatigue 2018; 116, 128-139.

Prasannavenkatesan R, McDowell D. Polycrystal plasticity modeling of cyclic residual stress relaxation in shoot peened martensitic gear steel. J Engng Mater Tech 2010; 132; 031011-1-031011-8.

Qylafku G, Azari Z, Kadi N, Gjonaj M, Pluvinage G. Application of a new model proposal for fatigue life prediction on notches and key-seats. Int J Fatigue 1999; 21; 753-760.

Siebel E, Pfender M. Weiterentwicklung der Festigkeitsrechniung bei schwingender Beanspruch. Stahl und Eisen 1947, Bd 66/67; 318-321.

Siebel E, Stieler M. Ungleichformige Spannungverteilung bei schwingender Beanspruchung. VDI-Z 1955; 97; 121-126.

Siebel E, Gaier M, Untersuchungen über den Einfluß der Oberflächenbeschaffenheit auf die Dauerschvingfestigkeit metallischer Werkstoffe. VDI-Z 1956; 98; 1715-1924.

Sines G. Behavior of metals under complex static and alternating stresses. in Metal Fatigue, Ed by G Sines and JL Waisman, McGraw-Hill 1959.

Skallerud, B. Constitutive modeling of cyclic plasticity and some implications for the computation of biaxial low cycle fatigue. Eng Fracture Mech 1992; 41, 753-769.

Suhr RW. The effect of surface finish on high cycle fatigue of a low alloy steel, in: Miller, K. J. and Rios, E. R. de los. (Eds.), The Behaviour of Short Fatigue Cracks, Mechanical Engineering Publications, 1986, 479-490.

Susmel L. The theory of critical distances: a review of its applications in fatigue. Eng Fracture Mech 2008; 75; 1706-1724.

Taylor D. Geometrical effects in fatigue: a unifying theoretical model. Int J Fatigue 1999; 21; 413-420.

Taylor D, Bologna P, Bel Knani K. Prediction of fatigue failure location on a component using a critical distance method. Int J Fatigue 2000; 22; 735-742.

Taylor D, Clancy OM. The fatigue performance of machined surfaces, Fatigue and Fracture of Engineering Materials and Structures, 1991, 14, 329-336.

Tomkins B. Fatigue crack propagation - An analysis. The Philosophical Magazine: A Journal of Theoretical Experimental and Applied Physics, Taylor & Francis, 1968, 18, 1041-1066.

Tovo R, Livieri P. An implicit gradient application to fatigue of complex structures. Eng Fract Mech 2008; 75; 1804-1814.

Zenner H, Kleemann U. Berechnung der Dauerschwingfestigkeit bei biaxialen Mittelspannungen, Materialwissenschaft und Werkstofftechnik, 2006, 37, 881-886.

Ås SK, Skallerud B, Tveiten BW, Holme B. Fatigue life prediction of machined components using finite element analysis. Int J Fatigue 2005; 27; 1590-1596.

Ås SK, Skallerud B, Tveiten BW. Surface roughness characterization for fatigue life prediction using finite element analysis. Int J Fatigue 2008; 30; 2200-2209.

Ås, S. Fatigue life prediction of an aluminium alloy automotive component using finite element analysis of surface topography, Norwegian University of Science and Technology, 25:2006.